X-ray Absorption Fine Structure Characterization of the Local Structure of Fe in Fe−ZSM-5

Sun Hee Choi,† Benjamin R. Wood, Jason A. Ryder, and Alexis T. Bell*

Department of Chemical Engineering, University of California, Berkeley, California 94720-1462

Received: January 31, 2003; In Final Form: May 22, 2003

The local structure of Fe in Fe−ZSM-5 prepared by solid-state exchange was investigated with XAFS. Fe K-edge spectra were taken at liquid nitrogen temperature for samples with Fe/Al ratios of 0.33, 0.66, and 0.80. The radial structure function (RSF) of He- and CO-pretreated Fe−ZSM-5 shows two main peaks, one at 1.6 Å and the other at 2.5 Å. To interpret the origin of these peaks, RSFs were simulated for a number of mono- and di-iron structures obtained from quantum chemical calculations. By this means, the peak in the RSF at 1.6 Å is clearly identified with backscattering from O atoms coordinated to an Fe atom. The peak at 2.5 Å has been previously ascribed to Fe−Fe scattering and has been used to argue for the presence of di-iron−oxo species; however, the origin of this peak and its interpretation remains an open question. The imaginary part of the Fourier transformed data for the peak at 2.5 Å has the same characteristics as that generated theoretically for Fe−Al backscattering and is distinctly different from that generated theoretically for Fe−Fe backscattering. This evidence strongly suggests that the iron in Fe−ZSM-5 is present as isolated cations associated with framework aluminum. Further evidence for such a structure is the absence of any change in the magnitude of the peak near 2.5 Å with sample treatment. The RSFs and the information obtained from curve-fitting demonstrate that the structure of Fe in Fe−ZSM-5 does not change significantly with Fe/Al ratio. For both He- and CO-pretreated sample, the Fe−O coordination number is about 4 and correspondingly the Fe−Al coordination number is about 1, regardless of Fe/Al ratio. Therefore, the structure of Fe in Fe−ZSM-5 is best described as either $Z^-[Fe(O)_2]^+$ or $Z^-[Fe(OH)_2]^+$, where Z^- represents the charge-exchange site in the zeolite. Upon O_2 pretreatment, a new feature appears at about 1.1 Å in the RSF, which may be due to a migration of some of the Fe into the zeolite framework. This interpretation is qualitatively consistent with the observed RSF for Fe−silicalite.

Introduction

Iron-exchanged ZSM-5 has been shown to be an active catalyst for a number of reactions. The decomposition of N_2O to N_2 and O_2 occurs over Fe−ZSM-5, the activity per Fe atom increasing with the degree of Fe exchange.[1−6] N_2O oxidation of benzene to phenol occurs with high selectivity over ZSM-5 containing small amounts of Fe, and has been attributed to a special form of adsorbed oxygen, designated α-O.[3−7] The latter species has also been shown to react with methane leading to the formation of methoxide species, which can be hydrolyzed quantitatively to form methanol.[3,7−11] A number of studies have been carried out aimed at understanding the effects of catalyst preparation and pretreatment on the structure of Fe in Fe−ZSM-5 and relating this information to catalyst activity.[12−21] It has been shown that the nature of the Fe species in Fe−ZSM-5 depends on the method of ion-exchange and the type of catalyst pretreatment. Formally, the electronic state of iron is either +2 or +3, depending strongly on the conditions of pretreatment. The most difficult issue to address is the nuclearity of Fe once it is exchanged into the zeolite. A number of structures for iron have been proposed on the basis of evidence derived from X-ray diffraction, Fourier transformed infrared spectroscopy, solid-state NMR, electronic spin resonance, and X-ray absorption spectroscopy. Joyner et al. have concluded that Fe in Fe−ZSM-5 occurs in different forms, ranging from isolated metal ions to large oxide clusters and small oxygen-containing nanoclusters such as Fe_4O_4 and Fe_4O_3.[12] Binuclear iron clusters, such as $[HO−Fe−O−Fe−OH]^{2+}$, were first suggested by Sachtler and co-workers.[13,14] Marturano et al.[15,16] and Battiston et al.[17,18] have reported evidence for binuclear iron−oxo complexes and diferric(hydroxy)oxo-bridged complexes on the basis of EXAFS spectra of fully exchanged Fe−ZSM-5 (Fe/Al ≅ 1). These di-iron structures resemble the core unit in methane monooxygenase (MMO) and have and are characterized by an Fe−Fe distance of approximately 3 Å. Additional evidence for di-iron oxo species has been presented recently by Jia et al.[19] When the loading of Fe in Fe−ZSM-5 is such that Fe/Al < 1, isolated Fe species have been found as the principal species. Bell and co-workers have presented evidence for such structures based on infrared spectroscopy iron loadings such that Fe/Al < 0.6.[20,21] Kucherov and Shelef, using ESR, have reported the presence of isolated Fe species for Fe/Al < 0.15 in samples of $FeCl_3$-exchanged H−ZSM-5 that had then been calcined at 773 K.[22]

The aim of the present work was to establish the effects of Fe/Al ratio and pretreatment conditions on the speciation of iron in Fe−ZSM-5. Fe−ZSM-5 with Fe/Al ratios of 0.33 to 0.80 was prepared by solid-state exchange and was characterized by XANES and EXAFS. The interpretation of EXAFS data was aided by simulations of radial structure functions for iron-containing species proposed to exist in Fe−ZSM-5. The structure of the latter species was determined from quantum chemical calculations.

* Author to whom correspondence should be addressed. Tel: 510-642-1536. Fax: 510-642-4778. E-mail: bell@cchem.berkeley.edu.

† Present address: Pohang Accelerator Laboratory, Hyojadong, Namgu, Pohang 790-784, Republic of Korea.

10.1021/jp030141y CCC: $25.00
Published on Web 10/04/2003

Experimental Methods

Materials Preparation. Fe−ZSM-5 was prepared by solid-state exchange using $FeCl_3$. Na−ZSM-5 (Alsi-Penta, Si/Al = 25) was first converted to the ammonium form by aqueous exchange with ammonium nitrate. After drying, the resulting NH_4−ZSM-5 was transformed to H−ZSM-5 by calcination in air at 823 K for 8 h. The calcined H−ZSM-5 was then transferred to a glovebox and mixed with an appropriate amount of anhydrous $FeCl_3$ (Aldrich, 99.99%). The mixture was placed into a sealed reactor without exposure to air and the reactor was then heated from 298 to 583 K, the sublimation temperature of $FeCl_3$. Upon cooling to room temperature, the sample was removed from the reactor and washed repeatedly with deionized water to remove Cl^-. Three Fe−ZSM-5 samples were prepared for this study. The samples are denoted as Fe−ZSM-5(x) where x is the Fe/Al ratio.

X-ray Absorption Fine Structure Measurements. Prior to X-ray absorption measurements, the as-prepared material was pressed into a wafer held in a sample holder. The sample holder was then mounted in a specially designed spectroscopic cell, similar to that described by Jentoft et al.[23] Beryllium windows mounted at both ends of the cell permitted passage of the X-ray beam through the cell, while allowing the cell to be filled with gas or evacuated. After purging the cell in helium, one of the following pretreatments was performed on the sample: (1) heat in helium at 773 K for 2 h 20 min; (2) heat in 10% O_2 at 773 K for 2 h; and (3) heat in 4% CO at 773 K for 2 h. After pretreatment, the cell was purged with helium while it cooled to room temperature, was sealed, and then was evacuated to prevent beam loss due to gas scattering.

XAFS measurements were conducted on beam lines 4-2 and 4-3 of the Stanford Synchrotron Radiation Laboratory (SSRL). The radiation was monochromatized using a Si(111) double-crystal monochromator and the incident beam was detuned by 15% at 7111.2 eV (the K-edge of Fe) using a piezo-electric translator in order to minimize contamination of higher harmonics. To minimize noise, the sample was cooled by attaching the cell to a dewar filled with LN_2. The intensities of the incident and transmitted beams were monitored using separate ionization chambers, through which flowed pure N_2. At least four scans were taken of each sample to obtain good signal-to-noise ratios (S/N). For each sample, a reference spectrum of Fe foil was recorded simultaneously so that the energy in the spectrum of sample could be calibrated with respect to the K-edge energy of Fe metal, 7111.2 eV. In addition to the sample, the spectra of FeO, Fe_2O_3, Fe_3O_4, and Fe−silicalite were collected for use as references. Boron nitride, which is nearly transparent to the X-ray beam, was used to dilute the concentrated compounds.

XAFS Data Analysis. EXAFS (extended X-ray absorption fine structure) data were analyzed using the UWXAFS 3.0 package [24] and the FEFF 8 code,[25] licensed from the University of Washington. The detailed procedure for data analysis is described elsewhere.[26,27] The pre-edge background was removed by using a simple linear fit. The post-edge background function was approximated with a piecewise spline that could be adjusted so that the low-R components of pre-Fourier transformed data $\tilde{\chi}(R)$ were minimized. The interference function of the EXAFS data could be obtained from $\chi(E) = [\mu(E) - \mu_0(E)]/\Delta\mu_0(E)$ above the absorption edge E_0, where $\mu(E)$ is the absorption coefficient at energy E, $\mu_0(E)$ is the atomic-like absorption, and $\Delta\mu_0(E_0)$ is the jump at the edge. The scaled EXAFS function $k^3\chi(k)$ in momentum (k) space was Fourier transformed to obtain the radial structural function (RSF) in R space. A shell of interest in the RSF was back-Fourier transformed into momentum space. The Hanning windowsills window function was used to reduce the truncation effects from both forward- and inverse-Fourier transformations over a finite range. The reference materials used as standards for fitting the experimentally derived RSFs were generated with the FEFF 8 code and the Fourier-filtered data were fitted in momentum space. The amplitude reduction factor (S_0^2) was taken to be 0.76 for Fe, and was determined by fitting the experimental RSF of an Fe foil to that for metallic Fe generated with the FEFF 8 code.

Theoretical Methods. The structures of both isolated iron and di-iron species were determined from quantum chemical calculations.[28] For isolated iron sites, the Fe atom and a portion of the zeolite framework were represented by a 23−26-atom cluster. The portion of the cluster describing the zeolite contains an Al atom in the T12 site of the framework surrounded by shells of O and Si atoms. The terminal Si atoms are fixed in their crystallographic positions as reported by Olson et al.[29] Dangling bonds are terminated by H atoms located 1.5 Å from each terminal Si atom o-oriented in the direction of the next T (tetrahedral) site. The anionic cluster is charge-compensated by a metal−oxo species, $[FeO]^+$, $[FeO_2]^+$, or $[Fe(OH)_2]^+$, placed between two of the four O atoms surrounding the Al atom. To represent a di-iron species, the two Fe atoms and the associated portion of the zeolite framework were represented by a 40−46-atom cluster terminated in a manner similar to that used for the cluster describing an isolated Fe cation.[30] The portion of the cluster describing the zeolite contains two Al atoms located in the T11 sites of a flat, six-membered ring (T10, T10, T11, T12, T12, T11) located at the intersection of the straight and sinusoidal channels within the ZSM-5 unit cell. Three di-iron species considered were $[HOFe(OH)_2FeOH]^{2+}Z^-$, $[Fe(OH)_2Fe(OH)_2]^{2+}Z^-$, and $Z^-[Fe(O_2)Fe]^{2+}Z^-$.

Quantum chemical calculations of the geometries were performed using nonlocal, gradient-corrected density-functional theory (DFT).[31] To represent the effects of exchange and correlation, Becke's 3-parameter exchange functional and the correlation functional of Lee, Yang, and Parr (B3LYP) were used.[32,33] 6-31G or double-ζ level were used for all atoms, with the exception of Fe. To describe Fe, the energy-consistent pseudopotentials of Stuttgart and Bonn were used in the small-core approximation.[34] Polarization functions were added to all atoms, with the exception of terminal H groups. No corrections were made for basis-set superposition error. All calculations were carried out using the Jaguar 4.0 suite of programs (Schrödinger, Inc.) and Gaussian 98.[35,36] With the exception of the terminal Si atoms, all of the atoms in the cluster were allowed to relax during the course of these calculations. The atomic coordinates for each mono- and di-iron species, determined from the quantum calculations, were then used to generate the theoretical EXAFS function $\chi(k)$. The FEFF 8 code was used for this purpose. Similar to the analysis of experimental data, the power-scaled theoretical EXAFS function, $k^3\chi(k)$, was Fourier transformed to obtain the RSF of a particular structure.

Results

Simulations of Mono-iron and Di-iron Cations. Simulated RSFs are presented in Figure 1 for an isolated Fe cation associated with one or two nonframework O atoms, or two OH groups. These three structures are designated $Z^-[FeO]^+$, $Z^-[Fe(O)_2]^+$, and $Z^-[Fe(OH)_2]^+$, where Z^- represents the zeolite framework. The RSF for each of these structures exhibits a peak between 1 and 2 Å, a peak between 2 and 3 Å, and a pair of overlapping peaks centered near 3 Å. Calculations made using the FEFF 8 code show that the first of these features is

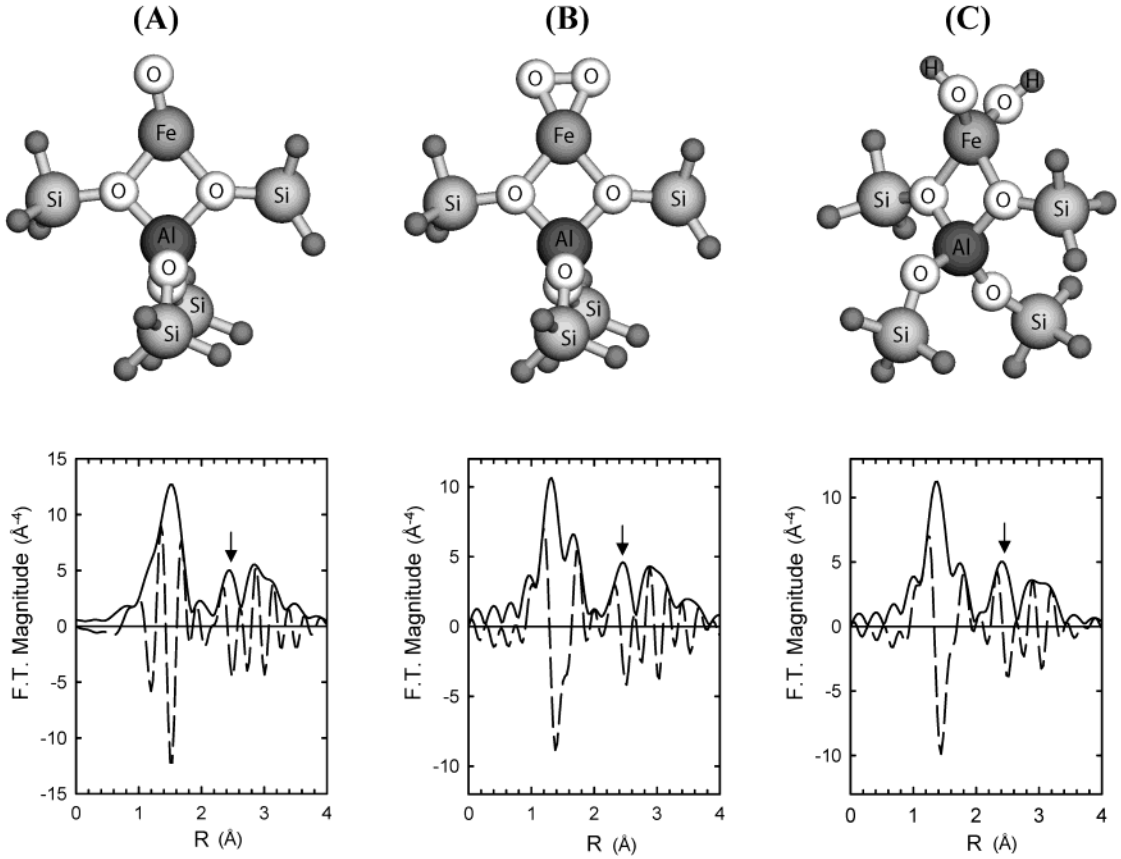

Figure 1. Fourier transforms of theoretical data for isolated iron species in Fe−ZSM-5. The imaginary parts of Fourier transformed data are plotted as dashed lines. (A) $Z^-[FeO]^+$, (B) $Z^-[Fe(O)_2]^+$, (C) $Z^-[Fe(OH)_2]^+$ where Z^- represents the zeolite framework.

TABLE 1: Distances between an Absorber Fe and Different Backscatterers in the Theoretical Structures of Figures 1 and 2

structure		distances (Å)			
		Fe−O	Fe−Al	Fe−Fe	Fe−Si
Figure 1 (A)	$Z^-[FeO]^+$	1.58, 1.90, 1.92	2.76		3.26, 3.27
(B)	$Z^-[Fe(O)_2]^+$	1.74, 1.79, 1.92, 1.94	2.75		3.24, 3.32
(C)	$Z^-[Fe(OH)_2]^+$	1.80, 1.81, 1.94, 2.00	2.79		3.27, 3.34
Figure 2 (A)	$Z^-[HOFe(OH)_2FeOH]^{2+}Z^-$	1.73, 1.91, 1.91, 2.03, 2.03	2.73	2.78	3.32, 3.33
(B)	$Z^-[Fe(OH)_2Fe(OH)_2]^{2+}Z^-$	1.83, 2.04, 2.04, 2.06	2.75	3.16	3.32, 3.33
(C)	$Z^-[Fe(O_2)Fe]^{2+}Z^-$	1.90, 1.91, 2.07, 3.03	2.69	2.90	3.22, 3.33

attributable exclusively to backscattering from O atoms bound to Fe. As noted in Table 1, the calculated Fe−O distances range from 1.58 to 2.00 Å. Similar calculations for the second peak in the RSF indicate that the dominant contribution is due to backscattering from the Al atom in the charge exchange site. Table 1 shows that the Fe−Al distance in the model structures range from 2.75 to 2.76 Å. The pair of overlapping peaks is attributable to Fe−Si backscattering. The Fe−Si distances in the model structures lie between 3.26 and 3.34 Å.

Figure 2 presents simulated RSFs for three di-iron hydroxo or oxo species ($Z^-[HOFe(OH)_2FeOH]^{2+}Z^-$, $Z^-[Fe(OH)_2$-$Fe(OH)_2]^{2+}Z^-$, $Z^-[Fe(O_2)Fe]^{2+}Z^-$). The Fe−O, Fe−Al, and Fe−Fe distances in these structures range are listed in Table 1. The RSF for each of the di-iron species is more complicated than that for an isolated Fe species because of the greater number and variety of the scattering paths associated with the former species. Once again, the FEFF 8 code was used to isolate the contributions to each peak in the RSF. For all three species, the peak appearing in the range of 1−2 Å can be assigned exclusively to Fe−O backscattering. The peak appearing in the region of 2−3 Å is now comprised of two dominant parts—one due to Fe−Al backscattering and the other due to Fe−Fe scattering. Figure 3 shows the contributions of Fe−Al and Fe−Fe backscattering to the RSF peak at 2−3 Å for $Z^-[HOFe$-$(OH)_2FeOH]^{2+}Z^-$. This figure demonstrates that the magnitude functions for the Fe−Al and Fe−Fe contributions are very similar, but that the imaginary portions of the RSF are distinguishable. When the two contributions are summed, the shape and position of the magnitude function is nearly identical to that of the magnitude functions of the individual contributions, but the imaginary part of the combined contribution to the RSF more nearly resembles that for Fe−Fe scattering.

The results presented in Figure 3 suggest that it would be difficult to determine whether a peak appearing in the RSF for a sample of Fe−ZSM-5 is due to Fe−Fe or Fe−Al backscattering alone or is due to a combination of the two types of backscattering, if attention is given only to the magnitude function. This would be particularly true if the Fe−Fe and Fe−Al distances were nearly the same. Identification of which contribution dominates can be made, though, by comparison of the imaginary part of the RSF for the peak in the region of 2−3 Å with that characteristic of Fe−Al, Fe−Fe, or Fe−Al and Fe−Fe backscattering. The ability to identify the backscattering element contributing to a given peak by observing the

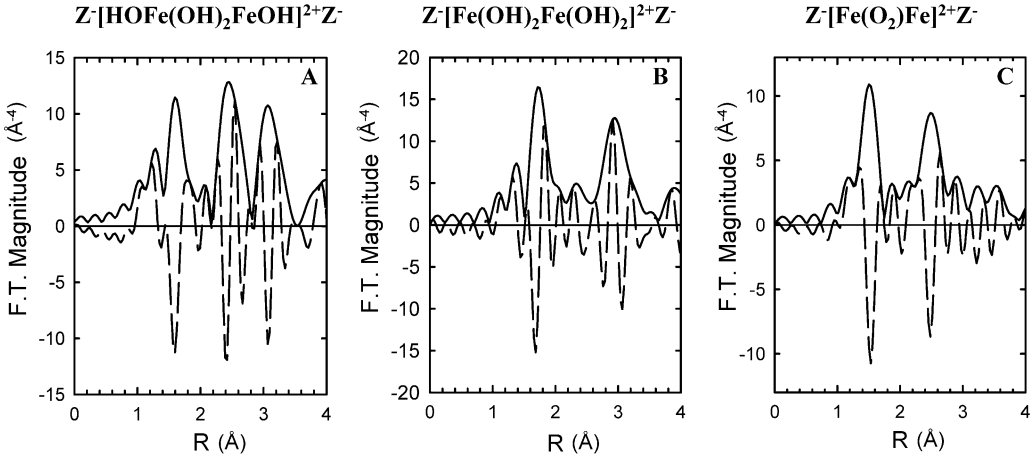

Figure 2. Fourier transforms of theoretical data for binuclear iron species in Fe−ZSM-5. The imaginary parts of Fourier transformed data are plotted as dashed lines. (A) $Z^-[HOFe(OH)_2FeOH]^{2+}Z^-$, (B) $Z^-[Fe(OH)_2Fe(OH)_2]^{2+}Z^-$, and (C) $Z^-[Fe(O_2)Fe]^{2+}Z^-$, where Z^- represents the zeolite framework.

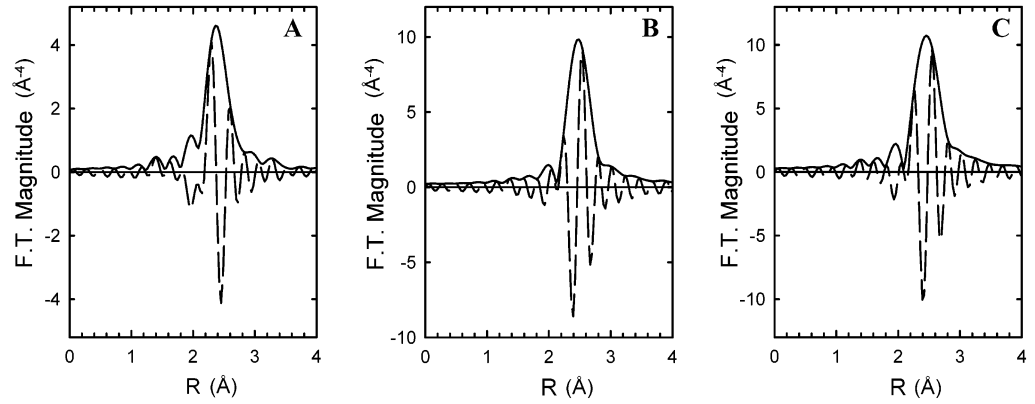

Figure 3. k^3-weighted Fourier transformation about the Fe K-edges of theoretical data for (A) Fe−Al pair, (B) Fe−Fe pair, and (C) combined contribution of Fe−Al and Fe−Fe pairs. The imaginary parts of Fourier transformed data are plotted as dashed lines. The theoretical EXAFS $\chi(k)$ was generated with the FEFF 8 for the structure of $Z^-[HOFe(OH)_2FeOH]^{2+}Z^{-1}$ in Figure 2a.

imaginary portion of the Fourier transformed data is supported by the recognition that this function is a characteristic of the absorber−backscatter pair, independent of the distance between the absorber and the backscatterer or the coordination number of the backscatterer.[37,38]

XANES Spectra of Fe−ZSM-5. Peaks observed in the XANES region of an XAFS experiment are due to electronic transition from an inner level to the outer unoccupied levels caused by X-ray absorption. These features give information about the local electronic structure and coordination environment around an absorber. Fe K-edge XANES spectra have a weak pre-edge feature ~10 eV below the absorption edge. This feature originates from a $1s \rightarrow 3d$ transition which, while electric dipole forbidden by parity consideration, is observed experimentally as a weak pre-edge feature due to electric quadrupole coupling.[39]

Fe K-edge XANES spectra of Fe−ZSM-5 are shown in Figures 4 and 5 for different sample pretreatments. The spectrum of Fe−silicalite is also shown in these figures for comparison. Fe−silicalite has the structure of ZSM-5 with Fe substituting for Al and, thus, iron is tetrahedrally coordinated to lattice oxygen. The Fe−ZSM-5 samples pretreated in He and CO have very weak pre-edge peaks, while the pre-edge peak for the sample treated in O_2 is more intense; however, the latter peak is distinctly less intense than that for Fe−silicalite. The XANES of Fe−ZSM-5 (0.66) after each of the three pretreatments is similar to those of Fe−ZSM-5 (0.33) and Fe−ZSM-5 (0.80).

XANES also provides the edge position, which is defined as the energy giving the maximal slope in the rapidly rising portion of the absorbance versus energy plot. Since the edge energy is directly related to the binding energy of the ejected photoelectron during the absorption process, it moves to a higher energy as the oxidation state of the absorbing atoms increases. Table 2 shows the Fe K-edge energies of Fe−ZSM-5 treated under different conditions. The edge energies for different standards are also listed in this table for comparison. Fe−ZSM-5 samples pretreated with He and CO have similar edge energies regardless of Fe/Al ratios, while the edge energies of O_2-pretreated samples are higher by 1.3−2.2 eV. However, all samples have the edge energies in the range of 7117.5 (edge energy of FeO)−7122.5 (edge energy of Fe_2O_3) eV. Fe−silicalite has the same edge as Fe_2O_3.

EXAFS Measurements for Fe−ZSM-5. Figure 6 shows the RSF for Fe−silicalite. Only a single major feature is observed at 1.4 Å, together with a number of smaller features at higher radial distances. The appearance of this RSF is very similar to that for Fe−silicalite reported previously in the literature.[40] All authors agree that the peak at 1.4 Å is attributable to Fe−O backscattering.

Plots of $k^3\chi(k)$ for FeO, Fe_2O_3, and for Fe−ZSM-5(0.33) pretreated with He and O_2 are shown in Figure 7. The EXAFS functions for the samples of Fe−ZSM-5 pretreated in He and O_2 are entirely different from those for the references compounds, for which structures are well-known,[40,41] indicating that the environment of Fe in Fe−ZSM-5 is different from that of the reference compounds.

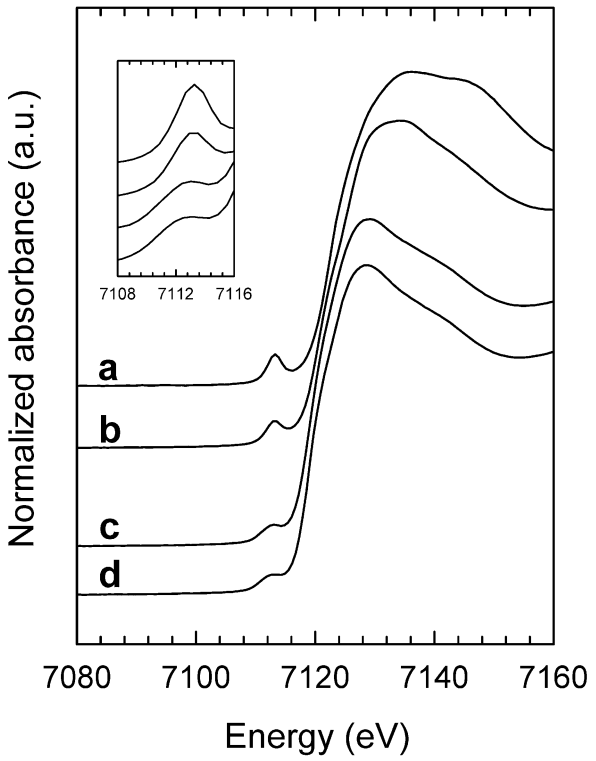

Figure 4. Fe K-edge XANES of (a) Fe−silicalite and Fe−ZSM-5 (0.33) (b) after O_2 pretreatment, (c) after He pretreatment, and (d) after CO pretreatment.

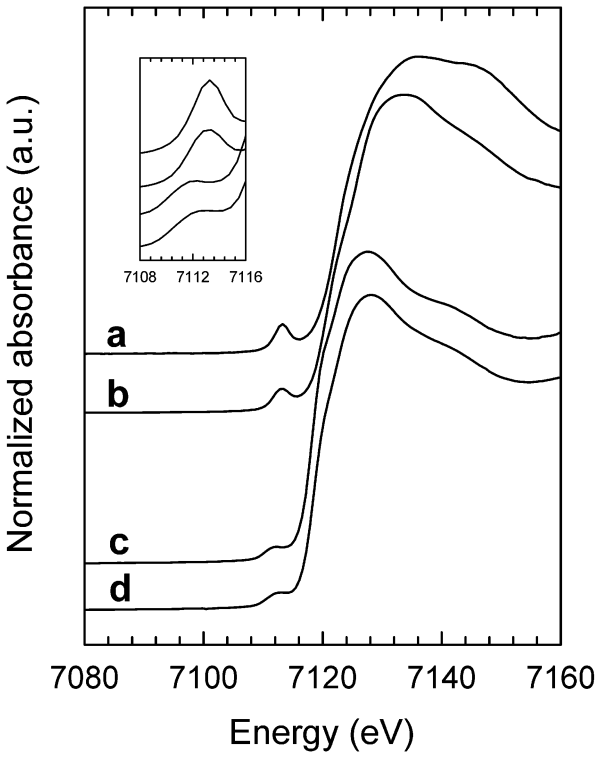

Figure 5. Fe K-edge XANES of (a) Fe−silicalite and Fe−ZSM-5 (0.80) (b) after O_2 pretreatment, (c) after He pretreatment, and (d) after CO pretreatment.

The RSF of Fe−ZSM-5(0.33) is displayed in Figures 8−10 for different pretreatments. Two distinct peaks are observed in the RSF when the sample is pretreated in He or CO—one at about 1.6 Å and the other at about 2.5 Å. The RSF of the O_2-pretreated sample shows the same two peaks together with a new peak at about 1.1 Å. As noted earlier, peaks in the region

TABLE 2: Fe K-edge Energies of the Reference Materials and Fe−ZSM-5

	edge energy (eV)[a]		
Fe foil	7111.2		
FeO	7117.5		
Fe_3O_4	7121.7		
Fe_2O_3	7122.6		
Fe−silicalite	7122.5		
Fe−ZSM-5(x)	He[b]	O_2[c]	CO[d]
$x = 0.33$	7119.3	7120.6	7119.1
$x = 0.66$	7118.8	7120.9	7118.4
$x = 1.00$	7118.7	7120.9	7118.7

[a] Precision, ±0.1 eV. [b,c,d] Pretreatment condition.

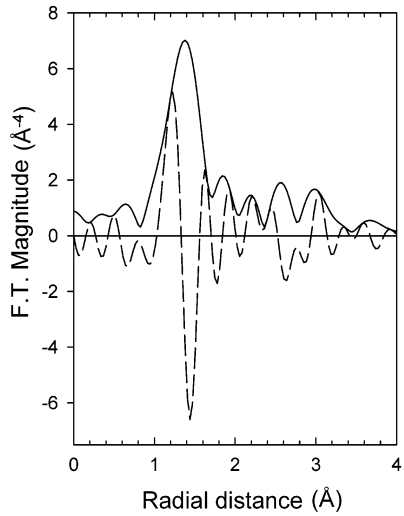

Figure 6. k^3-weighted Fourier transformation about the Fe K-edge of Fe−silicalite. The imaginary parts of Fourier transformed data are plotted as dashed lines.

of 1−2 Å can be attributed to backscattering from oxygen atoms coordinated to an iron absorber. The appearance of a new peak for Fe−O backscattering following O_2 pretreatment suggests that some of the Fe atoms have undergone a change their environment. The peak at 2−3 Å is still observed in the RSF for O_2-pretreated sample. As discussed above, this peak could be due to either Fe−Fe or Fe−Al backscattering.

The effects of sample pretreatment on the RSF of Fe−ZSM-5(0.33) and Fe−ZSM-5(0.80) are shown in Figures 11 and 12. Interestingly, the RSF of both Fe−ZSM-5 samples determined from EXAFS data taken prior to He pretreatment show two overlapping components in the region of 1−2 Å similar to what is seen after O_2 pretreatment. The principal difference is that the component centered near 1.6 Å is more intense when the sample is fresh. It is also evident that pretreatment in He, O_2, and then in CO has little effect on the intensities of the peaks at 1.6 Å and 2.5 Å.

Figures 13−15 display the effects of the Fe/Al ratio on the RSF of Fe−ZSM-5 after pretreatment in He, O_2, and CO, respectively. Comparison of Figures 13 and 15 demonstrates that the RSF following He and CO pretreatment are virtually the same, the only significant difference being that the ratio of the peak at 1.6 Å to that at 2.5 Å increases slightly with increasing Fe/Al ratio. Figure 14 shows that after O_2 pretreatment, the peaks at 1.1 Å and 2.5 Å are independent of Fe/Al ratio, whereas the peak at 1.6 Å increases with increasing Fe/Al ratio.

The Fourier-filtered EXAFS data were fitted using a model consisting of a single Fe absorber coordinated to one or two

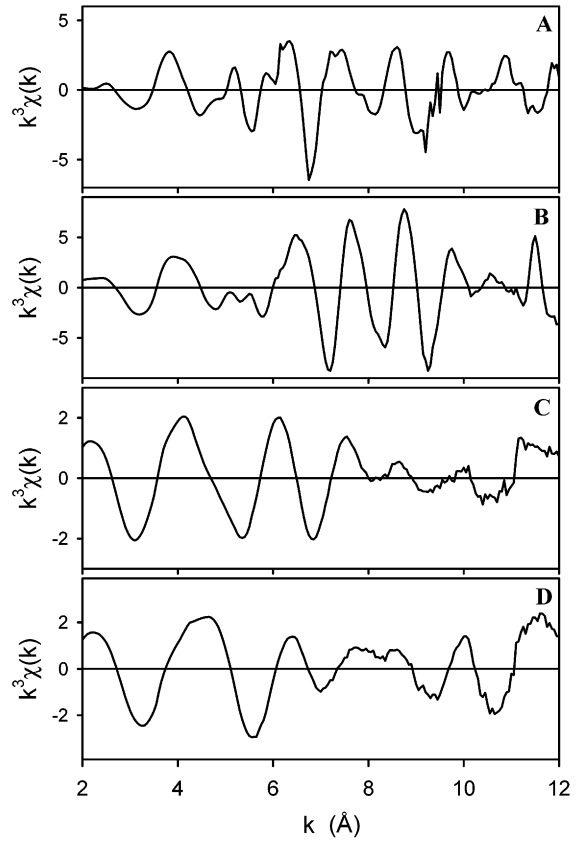

Figure 7. k^3-weighted EXAFS functions of (A) FeO, (B) Fe_2O_3, (C) Fe−ZSM-5 (0.33) pretreated with He, and (D) Fe−ZSM-5 (0.33) pretreated with O_2.

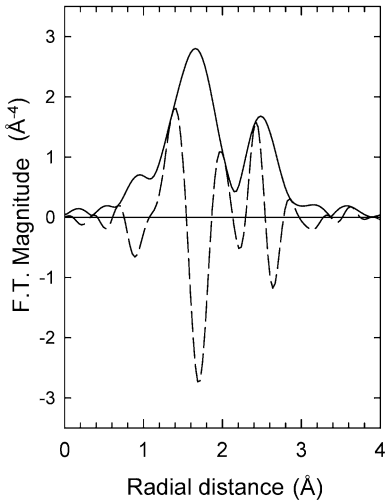

Figure 8. k^3-weighted Fourier transformation about the Fe K-edge of Fe−ZSM-5 (0.33) pretreated with He. The imaginary parts of Fourier transformed data are plotted as dashed lines.

shells of O atoms and a shell of Al atoms. The decision to consider Fe−Al and not Fe−Fe, or a combination of Fe−Al and Fe−Fe, backscattering was based on the shape of the imaginary portion of the RSF for the peak at 2.5 Å. Examination of Figures 1 and 3 shows that the shape of the imaginary portion of this peak is very similar to that for Fe−Al backscattering. This conclusion is further supported by the information presented in Table 3, which shows the positions of the positive and negative peaks of the imaginary part of the RSF relative to the position of the maximum in the magnitude of the peak at 2.5 Å. The values of ΔR for the He-pretreated sample of Fe−

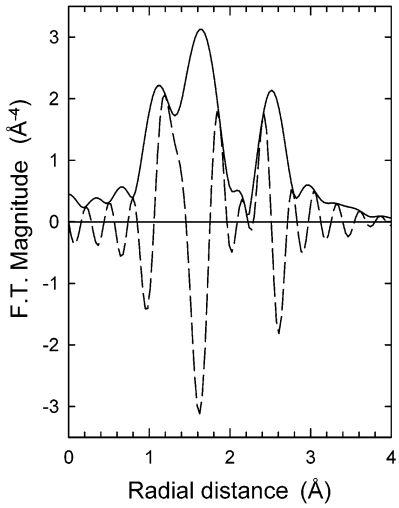

Figure 9. k^3-weighted Fourier transformation about the Fe K-edge of Fe−ZSM-5 (0.33) pretreated with O_2. The imaginary parts of Fourier transformed data are plotted as dashed lines.

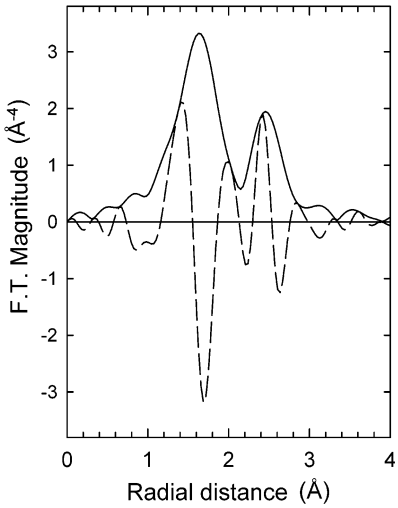

Figure 10. k^3-weighted Fourier transformation about the Fe K-edge of Fe−ZSM-5 (0.33) pretreated with CO. The imaginary parts of Fourier transformed data are plotted as dashed lines.

ZSM-5(0.33) agree much more closely with what is expected for Fe−Al backscattering, than with what is expected for Fe−Fe backscattering.

Only a single shell of O atoms was required to fit the data for samples pretreated in He and CO, but two shells of O atoms were required to fit the data for samples pretreated in O_2. As shown in Figure 16, a very good fit of the data in *k*-space could be obtained for all three types of sample pretreatment. The coordination number of the backscatterer and the distance of the backscatterer from the Fe absorber are presented in Table 4 for each of the samples and each of the pretreatments. The Debye−Waller factor and the edge energy shift for the best fit are also listed in Table 4, along with the *R*-factor, which defines the quality of the fit.

Table 4 shows that the coordination numbers and interatomic distances determined from a fit of the Fourier-filtered EXAFS data are virtually the same for samples of Fe−ZSM-5 pretreated in He or CO, independent of the Fe/Al ratio. In all cases, the coordination number of Fe with O is ∼4 and the Fe−O distance is ∼2.1 Å. Both the coordination number and the bond distance are similar to that for either $Z^-[Fe(O)_2]^+$ or $Z^-[Fe(OH)_2]^+$ (see Table 1 and Figure 1). The coordination number of Fe with Al ranges from 1.6 to 1.9, which is higher than that for either of

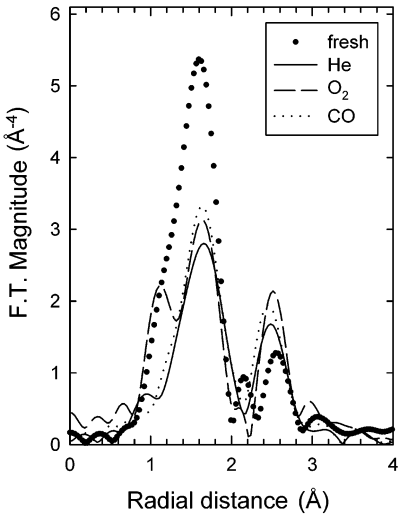

Figure 11. Comparisons of the magnitudes of Fourier transformed data for fresh Fe−ZSM-5 (0.33) with no pretreatment and the same catalysts pretreated with He or O_2 or CO.

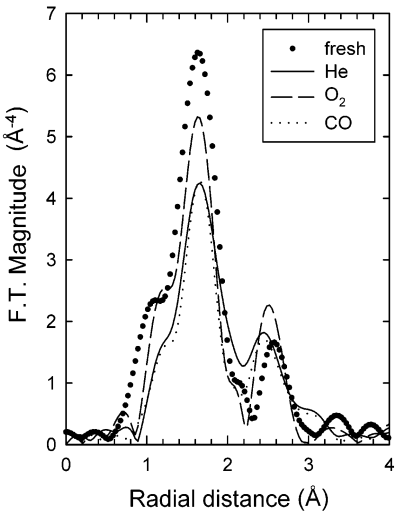

Figure 12. Comparisons of the magnitudes of Fourier transformed data for fresh Fe−ZSM-5 (0.80) with no pretreatment and the same catalysts pretreated with He or O_2 or CO.

the two model structures cited above. This apparent inconsistency could be a result of multiple scattering caused by the light O atoms lying along the scattering path between Fe and Al. An alternative interpretation is that the RSF peak at 2.5−3.0 Å may include a contribution from Fe−Si scattering. Since the scattering characteristics of Si and Al are very similar, it would not be possible to distinguish between these two elements. Nevertheless, the first of these interpretations is thought to be more nearly correct because the fitted Fe−Al distance is ∼2.9 Å, which is only slightly greater than that for the two proposed models of isolated Fe cations, and is noticeably smaller than that for the closest Si atom, 3.5 Å. Determination of whether $Z^-[Fe(O)_2]^+$ or $Z^-[Fe(OH)_2]^+$ represents the better model of the isolated iron site is not possible on the basis of the information given in Table 4. It is also noted that the simulated RSFs for these two structures are nearly the same, as can be seen from Figure 1.

Figures 9 and 14 clearly show that independent of the Fe/Al ratio of the sample, following O_2 pretreatment at 500 °C, a peak appears at 1.1 Å in the RSF. Table 4 demonstrates that in order to simulate this feature, it is necessary to include a second sphere of O atoms around Fe at a radius of ∼1.4 Å. This radius is

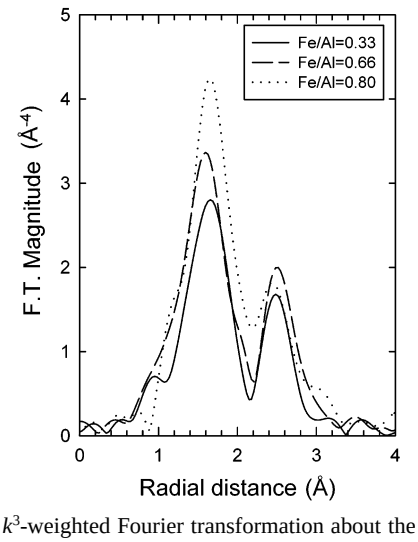

Figure 13. k^3-weighted Fourier transformation about the Fe K-edges of Fe−ZSM-5 with different Fe/Al ratios, which were pretreated with He.

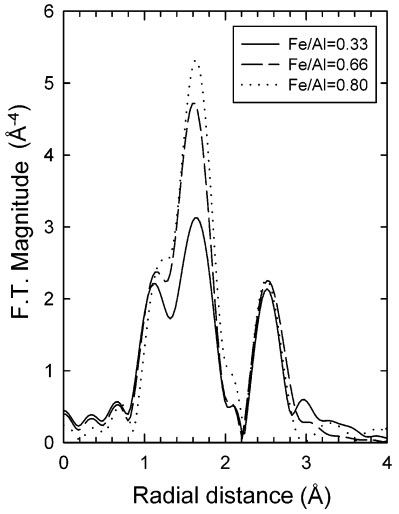

Figure 14. k^3-weighted Fourier transformation about the Fe K-edges of Fe−ZSM-5 with different Fe/Al ratios, which were pretreated with O_2.

considerably smaller than that associated with any type of extraframework Fe considered in this study. It is noted, however, that the RSF peak for Fe−O backscattering occurs at 1.4 Å when Fe is in the framework of the zeolite, as occurs in Fe−silicalite (see Figure 6). This suggests that upon O_2 pretreatment a part of the extraframework Fe may become incorporated into the framework. Since Fe in Fe−silicalite would be expected to have a more nearly tetrahedral environment than Fe present outside the framework as $[FeO_2]^+$ or $[Fe(OH)_2]^+$, the proposed interpretation would be consistent with the observed increase in the intensity of the pre-edge peaks in the XANES portion of the data upon O_2 pretreatment, seen in Figures 4 and 5.

Discussion

The appearance of both $k^3\chi(k)$ and the RSF for the samples reported here differ significantly from those reported by Marturano et al.,[15,16] as do the conclusions about the local environment of Fe. These authors prepared samples of Fe−ZSM-5 by passing a He stream containing $FeCl_3$ vapor through a bed of H−ZSM-5. The as-prepared material was then washed and calcined in either O_2 or He at 873 K. Analysis of the EXAFS data for the air-calcined sample led to the conclusion that a majority of the Fe is present as binuclear hydroxo−iron

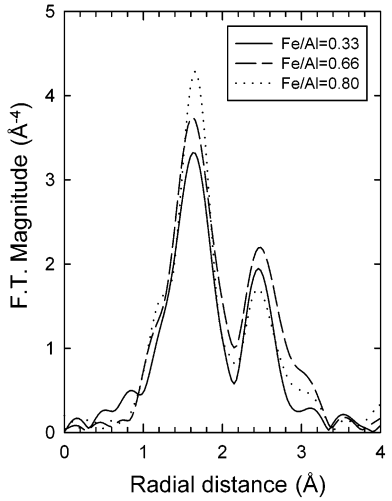

Figure 15. k^3-weighted Fourier transformation about the Fe K-edges of Fe−ZSM-5 with different Fe/Al ratios, which were pretreated with CO.

TABLE 3: Characteristics of the Imaginary Parts of the Fourier Transformed Data for the Peak at 2−3 Å

	ΔR[a]				
peak	Fe−ZSM-5 pretreated with He	Fe−Al scattering[b]	Fe−Fe scattering[c]	combined scattering of Fe−Al and Fe−Fe[d]	Fe−Al scattering[e]
1(positive)	−0.061	−0.061	−0.245	−0.184	−0.061
2(negative)	0.153	0.092	−0.092	−0.061	0.092
3(positive)	0.368	0.246	0.061	0.092	0.245
4(negative)			0.184	0.245	

[a] Difference in radial distance between the position at maximum intensity in the magnitude of Fourier transformed data and the one at either maximum or minimum in the imaginary parts. [b,c,d] Calculated for the structure of $Z^-[HOFe(OH)_2FeOH]^{2+}Z^-$. [e] Calculated for the structure of $Z^-[Fe(O)_2]^+$.

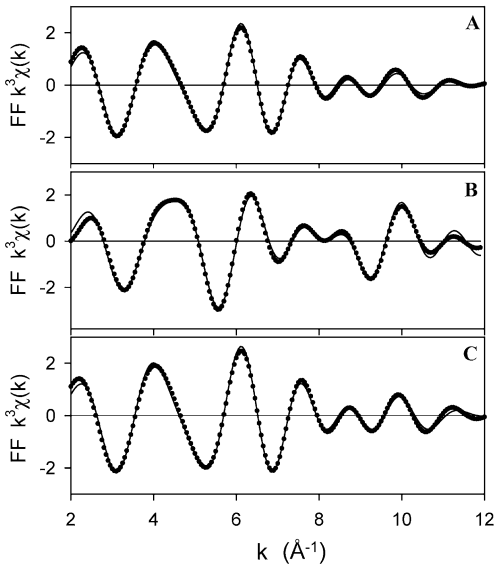

Figure 16. Fourier-filtered EXAFS data (solid line) and their best-fits (dots) of Fe−ZSM-5 (0.33) pretreated with (A) He, (B) O_2, and (C) CO.

clusters. If the calcination was carried out in He, evidence was found for the formation of Fe_3O_4 clusters, in addition to binuclear hydroxo−iron clusters.

The differences found in this study and that of Marturano et al. can be attributed to the manner of Fe−ZSM-5 preparation.

TABLE 4: Fe K-edge EXAFS Least-Square Fitting Results for Fe−ZSM-5 with Different Fe/Al Ratios Pretreated under Different Conditions

pretreatment	shell	N[a]	R (Å)[b]	σ^2 ($\times 10^{-3}$Å)[c]	ΔE_0 (eV)[d]	R-factor
Fe−ZSM-5 (0.33)						
He	O	3.5	2.14	15.8	2.2	0.0087
	Al	1.6	2.90	7.0	−2.2	
O_2	O	0.4	1.38	6.6	5.2	0.0148
	O	1.7	2.04	6.5	5.2	
	Al	1.4	2.92	4.2	6.1	
CO	O	3.9	2.12	14.8	0.43	0.0090
	Al	1.5	2.87	4.6	−4.4	
Fe−ZSM-5 (0.66)						
He	O	4.5	2.08	18.2	0.32	0.0417
	Al	1.1	2.88	1.8	−1.1	
O_2	O	0.4	1.40	5.3	3.2	0.0037
	O	2.4	2.02	4.9	3.2	
	Al	1.9	2.92	6.4	6.3	
Fe−ZSM-5 (0.80)						
e	O	4.6	2.11	12.9	−1.1	0.0159
	Al	1.9	2.82	5.3	−14.2	
O_2	O	0.4	1.44	7.7	4.1	0.0159
	O	2.4	2.03	3.8	4.1	
	Al	1.6	2.92	4.4	5.6	
CO	O	3.8	2.09	11.2	−1.3	0.0418
	Al	1.6	2.85	6.6	−9.7	

[a] Coordination number (±10%). [b] Interatomic distances (±0.02Å). [c] The Debye−Waller factor. [d] The energy shift. [e] R-factor gives a sum-of-squares measures of the fractional misfit, which is defined as $R = \{\sum_{i=1}^{N}\{[\mathrm{Re}(f_i)]^2 + [\mathrm{Im}(f_i)]^2\}/\sum_{i=1}^{N}\{[\mathrm{Re}(\tilde{\chi}_{\mathrm{data}}(k_i))]^2 + [\mathrm{Im}(\tilde{\chi}_{daai}(k_i))]^2\}$, where $f_i = \tilde{\chi}_{\mathrm{data}}(k_i) - \tilde{\chi}_{\mathrm{model}}(k_i)$.

The sample preparation method used by Marturano et al. was attempted in the early phase of this work but was abandoned after observation that the exchange of $[FeCl_2]^+$ for H^+ does not occur uniformly throughout the zeolite bed, but instead as a moving front. Since we were interested in achieving Fe/Al ratios of less than 1.0, we chose, instead to mix the appropriate amount of $FeCl_3$ with the H−ZSM-5 and then heat the solid mixture. This approach produced a solid of uniform color, independent of the Fe/Al ratio. It is conceivable, therefore, that a portion of the samples prepared by Marturano et al. had an Fe/Al ratio of more than one, while the balance had a ratio of less than one. Such a situation could still lead to a measured Fe/Al ratio of close to unity, but it would be more conducive to the association of the Fe atoms during washing and calcination, as was, in fact, demonstrated by Marturano et al. We believe that the sample preparation procedure used in the present study led to a more uniform distribution of Fe, and, hence, to the formation of isolated $[FeO_2]^+$ or $[Fe(OH)_2]^+$ structures. This view is supported by the observation that the RSFs of Fe−ZSM-5 with Fe/Al ratios between 0.33 and 0.80 are essentially the same (see Figures 14−16). We note further that the appearance of the RSFs for all of the He- and CO-pretreated samples of Fe−ZSM-5 reported here are qualitatively similar to that for the sample of Fe−ZSM-5 prepared by Marturano et al. and observed after sublimation, but before washing and calcinations, in which all of the Fe occurred in isolated cation structures, i.e., $[FeCl_2]^+$. We also note that the appearance of the RSF for Fe−ZSM-5 following sublimation, air exposure, washing, and air calcinations reported in Figure 8 of Marturano et al. is very similar to the simulated RSF for $Z^-[HOFe(OH)_2FeOH]^{2+}Z^-$, shown in Figure 2a. This suggests that the method of sample preparation used by Marturano et al. did, in fact, produce binuclear hydro−iron clusters. Since Battiston et al.[17,18] used a procedure for the preparation of ZSM-5 that was identical to that used by Marturano et al., their conclusion that iron is present as dinuclear clusters is plausible.

Joyner et al. have also investigated the structure for Fe−ZSM-5 and the effect of treatment with EXAFS.[12] For all EXAFS fits of sample prepared by an aqueous exchange method, they have considered the contributions of Fe−Fe and Fe−Si, as well as that of Fe−O scattering. Although the authors mentioned that the EXAFS spectrum of their as-prepared sample shows evidence for isolated iron atoms, the least-squares fitting results give an Fe−Fe coordination number of 1.4. The presence of Fe−Fe coordination is an indication that the iron is not in isolated state any more. With IR and EXAFS fitting results, they have concluded that an activation at high temperature leads to formation of small metal−oxo clusters in Fe-ZSM-5. Peaks of higher shell in all RSFs are clearly observed regardless of preparation method and sample treatment, but, the peaks are not properly identified. According to our calculation of theoretical structure for Fe−ZSM-5, an iron is more closely positioned to an aluminum atom rather than to a silicon atom (see Table 1). It is more reasonable, therefore, to adopt Fe−Al scattering instead of Fe−Si for the EXAFS least-squares fits.

Conclusions

The local structures of Fe in Fe−ZSM-5 with Fe/Al ratios between 0.33 and 0.80 were investigated with XANES and EXAFS. The position of the edge energy for Fe lies between that observed for FeO and Fe_3O_4. The RSF is characterized by two principal features located at 1.6 and 2.5 Å, irrespective of pretreatment conditions. The first of these peaks is associated with Fe−O backscattering. Fourier analyses and EXAFS least-squares fits indicate that the second peak originates from Fe−Al backscattering, not from Fe−Fe backscattering as has been proposed previously. The iron in Fe−ZSM-5, therefore, is present as isolated iron cations. For He- and CO-pretreated samples, the structure of Fe in Fe−ZSM-5 is best described as $Z^-[Fe(O)_2]^+$ or $Z^-[Fe(OH)_2]^+$, where Z^- represents the charge-exchange site in the zeolite. This is also supported by the theoretical spectrum of such a structure. Oxygen pretreatment leads to the appearance of a peak at 1.1 Å. While a definitive assignment of this feature cannot be made, it is noted that its position is consistent with the migration of some of the extraframework Fe into framework positions. This interpretation is also consistent with the observation of an increase in the intensity of the pre-edge XANES feature, which is ascribed to movement of some of the Fe into a more nearly tetrahedral environment.

Acknowledgment. We acknowledge Prof. B. Gates and Dr. O. Alexeev for their assistance in the construction of the XAFS cells and in carrying out the first experiments at SSRL. The XAFS data were collected at the Stanford Synchrotron Radiation Laboratory, a national user facility operated by Stanford University on behalf of the U.S. Department of Energy, Office of Basic Energy Sciences. This work was supported by a grant from BP.

References and Notes

(1) Centi, G.; Generali, P.; dall'Olio; L.; Perathoner, S. *Ind. Eng. Chem. Res.* **2000**, *39*, 131.

(2) Panov, G. I.; Sobolev, V. I.; Kharitonov, A. S. *J. Mol. Catal.* **1990**, *61*, 85.

(3) Panov, G. I.; Uriarte A. K.; Rodkin, M. A.; Sobolev, V. I. *Catal. Today* **1998**, *41*, 365.

(4) El-Malki, E. M.; van Santen, R. A.; Sachtler, W. M. H. *Microporous Mater.* **2000**, *35*, 235.

(5) Sang, C.; Lund, C. R. F. *Catal. Lett.* **2000**, *70*, 165.

(6) Sang, C.; Land, C. R. F. *Catal. Lett.* **2001**, *73*, 73.

(7) Dubkov, K. A.; Sobolev, V. I.; Talsi; E. P., Rodkin, M. A.; Watkins, N. H.; Shiteinman, A. A.; Panov, G. I. *J. Mol. Catal. A* **1997**, *123*, 155.

(8) Sobolev, V. I.; Dubkov, K. A.; Panna, O. V.; Panov, G. I. *Catal. Today* **1995**, *24*, 251.

(9) Panov, G. I.; Sobolev, V. I.; Dubkov, K. A.; Parmon, V. N.; Ovanesyan, N. S.; Shilov, A. E.; Shteinman, A. A. *React. Kinet. Catal. Lett.* **1997**, *61*, 251.

(10) Knops-Gerrits, P. P.; Smith, W. J. *Stud. Surf. Sci. Catal.* **2000**, *130*, 3531.

(11) Knops-Gerrits, P. P.; Goddard, W. A., III. *J. Mol. Catal. A* **2001**, *166*, 135.

(12) Joyner, R.; Stockenhuber, M. *J. Phys. Chem. B* **1999**, *103*, 5963.

(13) Chen, H.-Y.; Sachtler, W. M. H. *Catal. Today* **1998**, *42*, 73.

(14) El-Malki, E.-M.; van Santen, R. A.; Sachtler, W. M. H. *J. Phys. Chem. B* **1999**, *103*, 4611.

(15) Marturano, P.; Drozdova, L.; Kogelbauer, A.; Prins, R. *J. Catal.* **2000**, *192*, 236.

(16) Marturano, P.; Drozdova, L.; Pirngruber, G.; Kogelbauer, A.; Prins, P. *Phys. Chem. Chem. Phys.* **2001**, *3*, 5585.

(17) Battiston, A. A.; Bitter, J. H.; Koningsberger, D. C. *Catal. Lett.* **2000**, *66*, 75.

(18) Battiston, A. A.; Bitter, J. H.; De Groot, F. M. F.; Overweg, A. R.; Stephan, O.; van Bokhaven, J. A.; Kooyman, P. J., van der Spek, C.; Vanko, G.; Koningsberger, D. C. *J. Catal*. **2003**, *213*, 251.

(19) Jia, J.; Sun, Q.; Wen, B.; Chen, L. X.; Sachtler, W. H. M. *Catal. Lett.* **2002**, *82*, 7.

(20) Lobree, L. J.; Hwang, I.-C.; Reimer, J. A.; Bell, A. T. *J. Catal.* **1999**, *186*, 242.

(21) Wood, B. R.; Reimer, J. A.; Bell, A. T. *J. Catal.* **2002**, *209*, 151.

(22) Kucherov, A. V.; Shelef, M. *J. Catal*. **2000**, *195*, 106.

(23) Jentoft, R. E.; Deutsch, S. E.; Gates, G. C. *Rev. Sci. Instrum*. **1996**, *67*, 2111.

(24) Stern, E. A.; Newville, M.; Ravel, B.; Yacoby, Y.; Haskel, D. *Physica B* **1995**, *208 & 209*, 117.

(25) Ankudinov, A. L.; Ravel, B.; Rehr, J. J.; Conradson, S. D. *Phys. Rev. B* **1998**, *58*, 7565.

(26) Choi, S. H.; Lee, J. S. *J. Catal.* **1997**, *167*, 364.

(27) Park, E. D.; Choi, S. H.; Lee, J. S. *J. Phys. Chem. B* **2000**, *104*, 5586.

(28) Ryder, J. A.; Chakraborty, A. K.; Bell, A. T. *J. Phys. Chem.* **2002**, *106*, 7059.

(29) Olson, D. H.; Kokotallo, G. T.; Lawton, S. L.; Meier, W. M. *J. Phys. Chem.* **1981**, *85*, 2238.

(30) (a) Rice, M. J.; Chakraborty, A. K.; Bell, A. T. *J. Catal*. **1999**, *186*, 222. (b) Rice, M. J.; Chakraborty, A. K.; Bell, A. T. *J. Catal*. **1999**, *194*, 278.

(31) Parr, R. G.; Yang, W. *Density-Functional Theory of Atoms and Molecules*; Oxford University Press: Oxford, 1989.

(32) Becke, A. D. *Phys. Rev. A* **1988**, *38*, 3098.

(33) Lee, C.; Yang, W.; Parr, R. G. *Phys. Rev. B* **1988**, *37*, 785.

(34) Dolg, M.; Wedig, U.; Stoll, H.; Preuss, H. *J. Chem. Phys.* **1987**, *86*, 866.

(35) Jaguar 4.0; Schrödinger, Inc.: Portland, OR, 2000.

(36) *Gaussian 98*; Gaussian Inc.: Pittsburgh, PA, 1998.

(37) Sayers, D. E.; Bunker, B. A. In *X-ray Absorption: Principles, Applications, Techniques of EXAFS, SEXAFS and XANES*; Koningsberger, D. C., Prins, R., Eds.; John Wiley & Sons: New York, 1988; p 211.

(38) Vaarkamp, M. *Catal. Today* **1998**, *39*, 271.

(39) Shulman, R. G.; Yafet, Y.; Eisenberger, P.; Blumberg, W. E. *Proc. Natl. Acad. Sci. U.S.A.* **1976**, *73*, 1384.

(40) (a) Axon, S. A.; Fox, K. K.; Carr, S. W.; Klinowski, J. *Chem. Phys. Lett.* **1992**, *189*, 1. (b) Patarin, J.; Tuiller, M. H.; Durr, J.; Kessler, H. *Zeolites* **1992**, *12*, 70. (c) Lewis, D. W.; Sankar, G.; Catlow, C. R. A.; Carr, S. W. *J. Phys. Chem*. **1995**, *99*, 2377. (d) Lewis, D. W.; Sankar, G.; Catlow, C. R. A.; Carr, S. W.; Thomas, J. M. *Nucl. Inst. Methods Phys. Res. B* **1995**, *97*, 44. (e) Berlier, G.; Spoto, G.; Bordiga, S.; Ricciardi, G.; Fisicaro, P.; Zecchina, A.; Rossetti, I.; Selli, E.; Forni, L.; Giamello, E.; Lamberti, C. *J. Catal*. **2002**, *208*, 64.

(41) Wyckoff, R. W. G. *Crystal Structures*, 2nd ed.; Interscience: New York, 1963; Vol. 1.